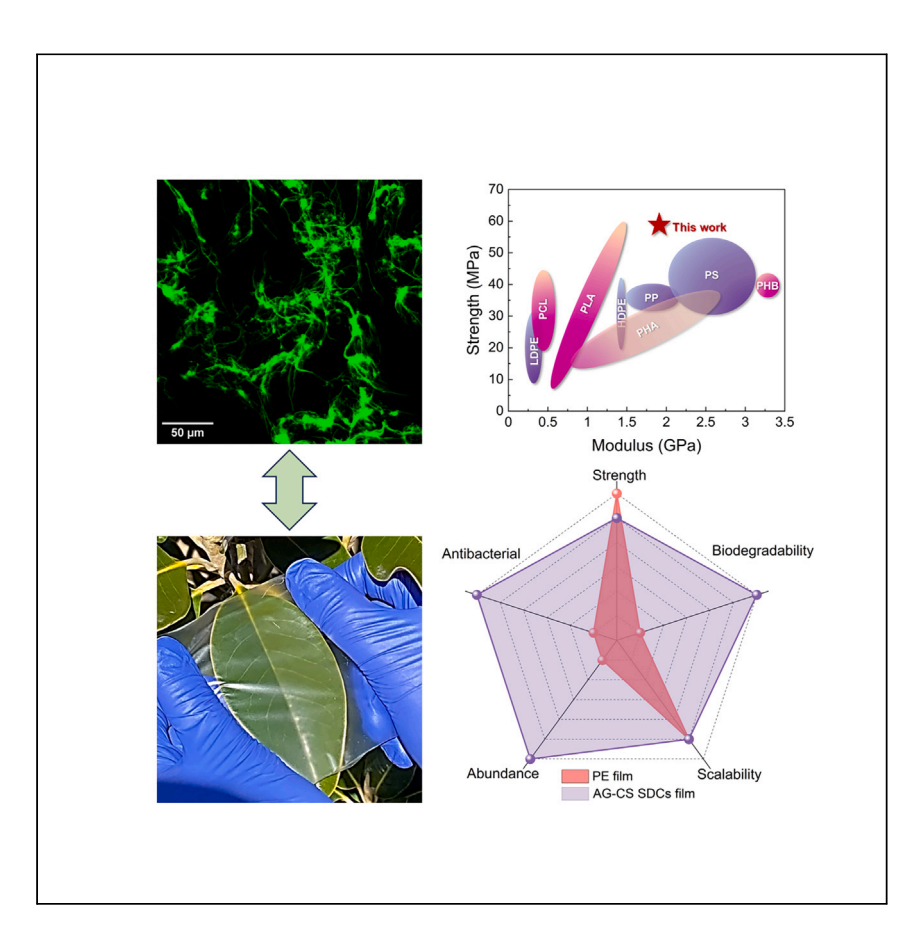


#### **Article**

# Hierarchically reinforced biopolymer composite films as multifunctional plastics substitute



Kotb and Velev report how the embedding of hierarchically fibrillated chitosan in an agarose matrix enables the formation of tough, transparent, antibacterial, and biodegradable composite films. Such reinforced biopolymer composites, made from renewable natural resources, could in the future serve as sustainable alternatives to synthetic petroleum-based plastics.

Yosra Kotb, Orlin D. Velev

odvelev@ncsu.edu

#### Highlights

Agarose films reinforced with fibrillar chitosan have outstanding properties

Chitosan is prepared in the form of hierarchically branched soft dendritic colloids

Biocomposite films are tough, transparent, bactericidal, and biodegradable

Films with improved properties could serve as synthetic polymer film replacements

Kotb & Velev, Cell Reports Physical Science 4, 101732

December 20, 2023 © 2023 The Authors. https://doi.org/10.1016/j.xcrp.2023.101732





#### **Article**

### Hierarchically reinforced biopolymer composite films as multifunctional plastics substitute

Yosra Kotb<sup>1</sup> and Orlin D. Velev<sup>1,2,\*</sup>

#### **SUMMARY**

The replacement of synthetic plastics with biodegradable alternatives made from abundant and sustainable raw materials is a challenge of high societal importance. We report a class of high-performance multifunctional composite films made of nano- and microscale reinforced naturally sourced biopolymers. These films are made of an agarose matrix reinforced with hierarchically branched soft dendritic colloids (SDCs) from chitosan. Owing to the highly entangled hierarchical network of the SDC nanofibrils, the reinforced composite has excellent performance with more than 4× higher toughness than non-reinforced agarose, high visible light transmittance, improved hydrostability, and remarkable bactericidal activity. Thus, these reinforced biopolymer composites could match or exceed the excellent mechanical, barrier, and optical properties of common synthetic polymer films. We also demonstrate the soil biodegradability of this composite material in a controlled environment. The results suggest a universal strategy for manufacturing natural-source composite materials that could serve as substitutes for petroleum-based plastics.

#### **INTRODUCTION**

Synthetic plastic materials and products are widely used in almost every aspect of modern life. Despite the enormous contribution of plastics to human well-being and convenience and society's prosperity, both the environment and human health are facing potential dangers from some forms of commonly used plastics. <sup>1–4</sup> Over the past three decades, the excessive production and consumption of fossil-oil-derived plastics have created large environmental and ecological challenges. In 2019, worldwide plastics production reached 368 million metric tons, of which less than 20% was recycled, with the rest being discarded in the environment or incinerated. <sup>5</sup> The accumulation of plastic waste on land and in oceans has proven to be detrimental to the earth's ecosystems and wildlife, as synthetic plastics may take hundreds of years to decompose and may create microplastics during degradation. <sup>6,7</sup> To limit the environmental damage, there is rapidly growing societal, industrial, and scientific interest in the formulation and properties of renewable plastics substitutes that are biodegradable and low cost. <sup>8–11</sup>

One of the most promising routes to replace petroleum-based plastics with sustainable alternatives is the use of biopolymers. <sup>12,13</sup> Common examples of such biopolymers include plant- and bacterial-derived cellulose, marine- and fungal-derived chitin, and animal-produced silk, which are based on resources that are abundant and renewable. <sup>14–18</sup> Nevertheless, performance limitations and high production



<sup>&</sup>lt;sup>1</sup>Department of Chemical and Biomolecular Engineering, North Carolina State University, Raleigh, NC 26795, USA

<sup>&</sup>lt;sup>2</sup>Lead contact

<sup>\*</sup>Correspondence: odvelev@ncsu.edu https://doi.org/10.1016/j.xcrp.2023.101732



costs have hindered the widespread use of such polymer substitutes, restricting them to mostly niche products that represent less than 1% of the plastics market. <sup>10,19–23</sup> Challenges related to thermal stability, brittleness, and processability of the biopolymer materials must be addressed, and their biodegradability and recyclability should be assessed, before they can secure a sizable foothold in the market. <sup>12</sup> One approach to the design of composite biopolymer materials with enhanced mechanical resilience and a range of other improved properties is to reinforce the biopolymer matrix with fillers with high aspect ratios, such as fibers. <sup>10,24–28</sup> It could be expected that the reinforcement strength and efficiency could be specifically improved by hierarchically branched fibrillar inclusions due to soft interface-induced extrinsic energy dissipation. <sup>29,30</sup>

We report a class of biopolymer-based composites reinforced by a hierarchical fibrillar network of soft dendritic colloids (SDCs) made of chitosan. SDCs are hierarchically structured particulates produced via scalable shear-driven polymer precipitation in a turbulent non-solvent medium. <sup>31,32</sup> Our previous studies demonstrated that sodium alginate SDCs can be used to efficiently form homocomposite hydrogels. <sup>33</sup> These hydrogels containing SDC networks showed synergistic properties with 3× higher storage modulus and 4× larger Young's modulus compared to pure molecular alginate gel. Separately, polyurethane SDCs were used to fabricate 3D scaffolds with tunable mechanical and morphological properties mimicking the soft human lung tissue for toxicological testing. <sup>34</sup>

The bulk biopolymer matrix used in this work is made of agarose (AG), which is a commonly used biopolymer extracted from red seaweed. AG has excellent film-forming properties due to its thermoreversible sol-gel transition when cooling below the gelling temperature. <sup>35,36</sup> The fibrillar reinforcement network that we embed in the AG matrix is made of chitosan (CS). CS is a biopolymer of particular interest for use in advanced polymeric alternatives. It is derived from chitin, which is the second most abundant biopolymer in nature and has drawn interest due to its biocompatibility, biodegradability, antibacterial activity, and solubility in mildly acidic solutions. <sup>37–40</sup> These two biopolymers have been previously investigated as molecular blends in hydrogels and films due to their chemical compatibility and have shown improved overall functional properties of the composite materials. <sup>41–46</sup>

We investigate the effectiveness of the reinforcement of the AG matrix with CS SDCs by characterizing the overall change in the mechanical performance of the resulting films. In addition, we evaluate a range of other properties that could be relevant in the use of such composite films as plastic substitutes, including optical transparency, surface hydrophobicity, biodegradability, and antibacterial activity.

#### **RESULTS AND DISCUSSION**

#### **Fabrication of CS SDCs**

The CS SDCs used in the reinforcement network for the composite films are fabricated using the process of liquid shear-driven precipitation under highly turbulent conditions that we previously developed and reported (Figure 1A). <sup>31,32</sup> In order to form and ionically crosslink the sheared CS fibrils, a solution of CS (3 wt %) is injected in a turbulently sheared medium containing citrate ions, which can effectively bind the protonated amine groups (NH<sub>3</sub><sup>+</sup>) on the CS backbone. This method of ionic precipitation rapidly forms stable hydrogel-like hierarchical fibrils. <sup>47,48</sup> The resulting "dendricolloids" or SDCs are characterized by hierarchical branching where the thicker central fiber core is surrounded by multidirectional micron-scale branches



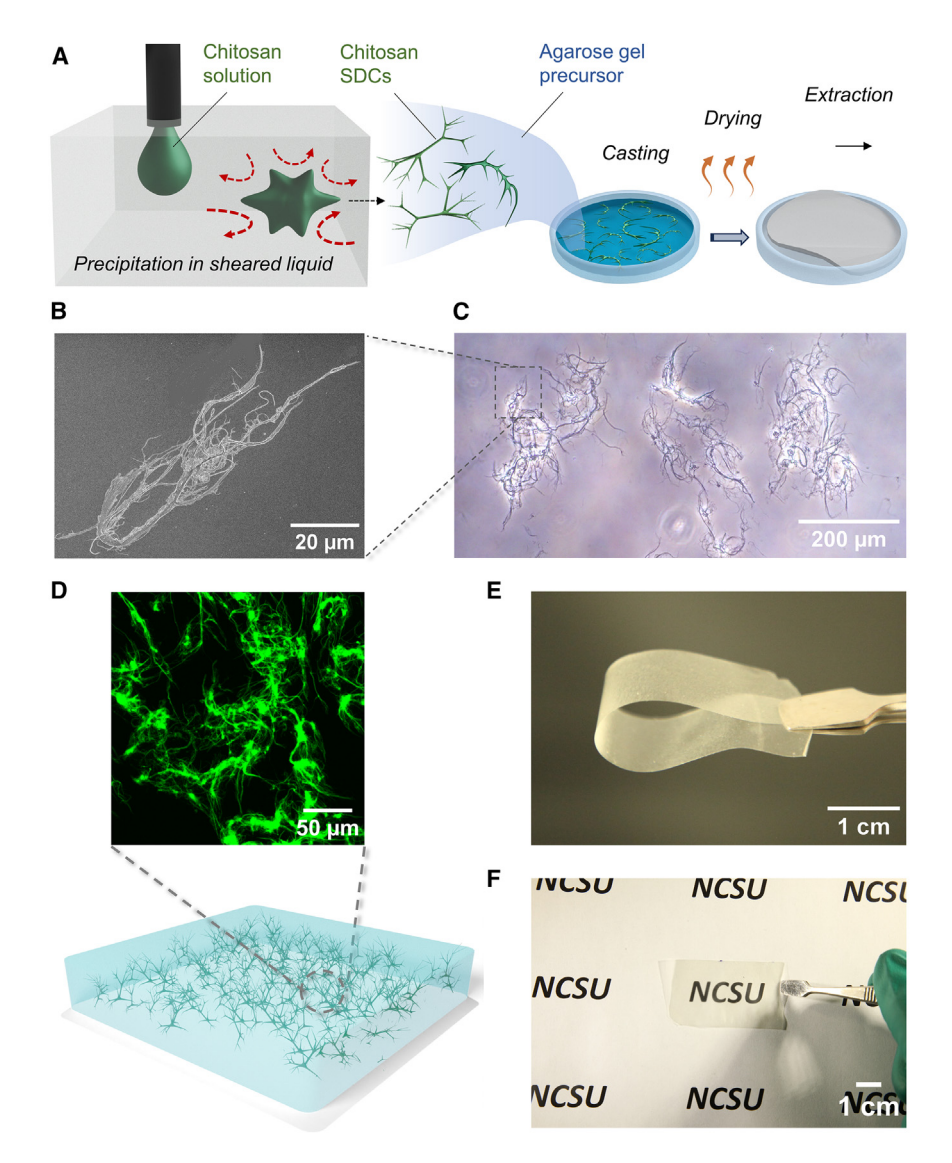


Figure 1. Fabrication of CS SDC particles and microstructural and macroscopic features of the composite films

- (A) Schematic illustration of the liquid shear-driven precipitation process. The polymer solution is injected in a turbulently sheared non-solvent medium producing the highly branched SDCs.
- (B) Scanning electron microscopy (SEM) image showing the morphology of one CS SDC particle.
- (C) Optical microscopy image showing a water-based suspension of CS SDCs.
- (D) Schematic illustration of the obtained composite film with a confocal microscopy image showing the CS SDCs forming an entangled 3D network inside the AG matrix.
- (E and F) Photographs of the AG-CS SDC 15 film (with 15% loading with SDC particles) showing the flexible nature of the composite and its transparency/translucency against printed text.

and nanofibrillar corona (Figure 1B). The fibers in the corona surrounding the SDCs are of micrometer scale in length and nanometer scale in diameter (Figure 1C). The SDCs have high surface area and high adhesivity of the nanofibers at their terminal branches. As shown earlier, this adhesivity is a result of the "gecko leg" effect—contact splitting combined with van der Waals adhesion present in dense nanofiber systems.<sup>31</sup> The SDCs have a strong propension for colloidal networks formation, as evidenced by the gel-like state of the CS SDC suspension (Figure S1).<sup>33</sup>



Composite films of varying thicknesses from AG with embedded CS SDCs were fabricated via solvent casting and drying as described in detail in the experimental procedures and supplemental information (Figure S2). Upon cooling, the AG solution forms a porous 3D physical gel network by the aggregation of the double helices of AG chains. When the CS SDCs are mixed inside the AG solution before gelation, the SDCs are embedded within the AG matrix, where they form an interconnected network (Figure 1D). After casting and drying, the films could be easily peeled from the molds for later use. The dried composite films are highly flexible and transparent with a slight haze (Figures 1E and 1F). The surfaces of these films appeared smooth without evident signs of internal clumping or agglomeration (Figure S2). To investigate the spatial distribution and networking of the CS fibrils dispersed inside the matrix, in some experiments, the SDCs were labeled with fluorescent dye, and their morphology in the dried films was visualized using confocal microscopy. The SDCs are seen as being homogeneously distributed and highly entangled inside the porous network of AG (Figure 1D; Figure S2).

#### Mechanical and optical properties

The incorporation of CS SDCs in the 3D porous network of AG leads to a major impact on the mechanical properties of the composite films in comparison to pure AG ones. In order to evaluate the effect of CS SDCs on the films' mechanical properties, we measured the uniaxial stress-strain response of films with different loadings of SDCs (Figure 2A, where the last number of a sample code denotes the wt % of the reinforcement). The tensile strength of the AG-CS SDC 5 films with a low content of 5% CS SDCs increased slightly compared to that of pure AG films, while, remarkably, the elongation at break doubled from  $\sim$ 4.5% to 10%. This increase in strength and elongation resulted in 1.7 × enhanced toughness for the AG-CS SDC 5 film (Figure 2B). For AG-CS SDC 30 films with higher CS SDC content (30 wt %), the tensile strength increased from 35 to 60 MPa. At the same content, the elongation at break and toughness were 17% and 7.2 MJ m<sup>-3</sup>, which represent 3.7-and 4.8-fold increases compared to pure AG film, respectively.

These results show that the addition of CS SDCs into the composite films enables one to achieve significantly improved mechanical performance. It is worth noting that the improved toughness is not associated with an increased stiffness, as the Young's moduli are relatively constant for the pure AG as well as the AG-CS SDC films. This reveals the ductile nature of the CS SDC reinforcement network, which does not impart rigidity and retains the flexibility of the AG matrix (Figure 2D). To analyze the effectiveness of reinforcement with SDCs in comparison to molecular mixtures, we prepared molecularly blended composite films by mixing AG and CS solutions at 15 wt % CS and heterogeneously crosslinking the film with NaCit. 49,50 As shown in Figure S3, the addition of 15% molecular CS improved the elongation at break of the film; however, the film had a much lower ultimate tensile strength. Compared to the composite film with CS SDCs at the same loading, the toughness and ultimate tensile strength decreased by 100% and 67%, respectively, for the films made by directly blending molecular CS and AG. This proves the efficacy of the SDC reinforcement network, which synergistically combines the benefits of molecular and microscale morphologies. In comparison with other reported films made of molecular blends of AG and CS, a previous study achieved a maximum tensile strength of 42 MPa and elongation at break of 17% with a film containing 50%-50% blend. 44 Another study showed a tensile strength and elongation of 6 MPa and 4.5%, respectively, using a film containing 40% AG and 60% CS. 42 In another work, a composite film containing 10% AG and 90% CS had a maximum strength of 19 MPa and elongation of 35%.<sup>51</sup> Compared to those studies, one can see that the SDC



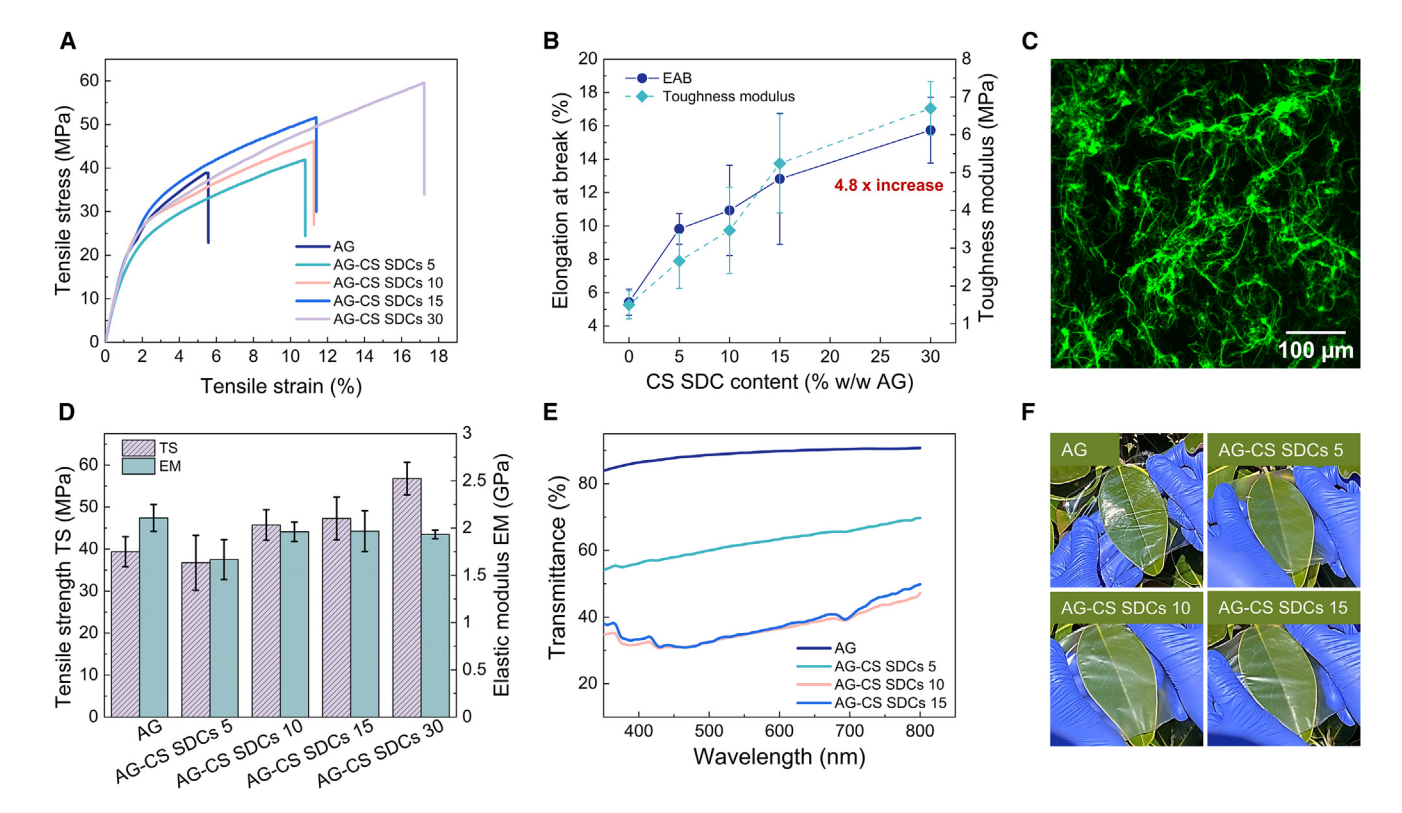


Figure 2. Optical and mechanical properties of the AG-CS SDC composite films

- (A) Tensile stress-strain curves of films reinforced with different contents of SDCs.
- (B) Comparison of the stretchability and toughness of the composite films with different contents of SDCs. Data are presented as mean  $\pm$  SD, n = 5.
- (C) Confocal laser scanning microscopy image showing the entangled CS SDC network embedded inside the AG matrix.
- (D) Comparison of the tensile strength and stiffness data of the composite films with different contents of CS SDCs. Data are presented as mean  $\pm$  SD, n = 5.
- (E) Light transmittance of the AG and composite films with CS SDCs within the range of 350–800 nm.
- (F) Photographs illustrating the optical translucency of the films containing SDCs.

reinforcement strategy offers a significant improvement in terms of enhanced mechanical performance using minimized content of the CS SDC particles.

Improving both strength and toughness is an essential requirement for most functional materials, although the two properties are commonly conflicting. <sup>52</sup> The composite film displays simultaneous enhancement in strength and toughness due to the SDC reinforcement mechanism. This effect can be attributed to the formation of a secondary physical network due to the entanglement of the SDC fibers inside the matrix (Figure 2C). <sup>33</sup> As the function of the AG is mostly to provide the continuous matrix surrounding the SDCs and to distribute the stresses among individual fibers, we conclude that there is an effective load transfer between the matrix and the SDC fibrils during stretching, which leads to an increased overall strength for the composite. <sup>10</sup> The high interfacial adhesion and formation of hydrogen bonds between the AG matrix and CS SDCs lead to enhanced fiber-matrix adhesion during stretching, which increases the toughness of the composite.

Optical transparency is a desirable property for biopolymer-based composites in applications such as food packaging or as substrates for wearable flexible electronics. The light transmittance of the films was characterized using UV-visible (UV-vis) spectroscopy (Figure 2E). The pure AG films were visually transparent and clear and had high transmittance (~90%) across the wavelength range of



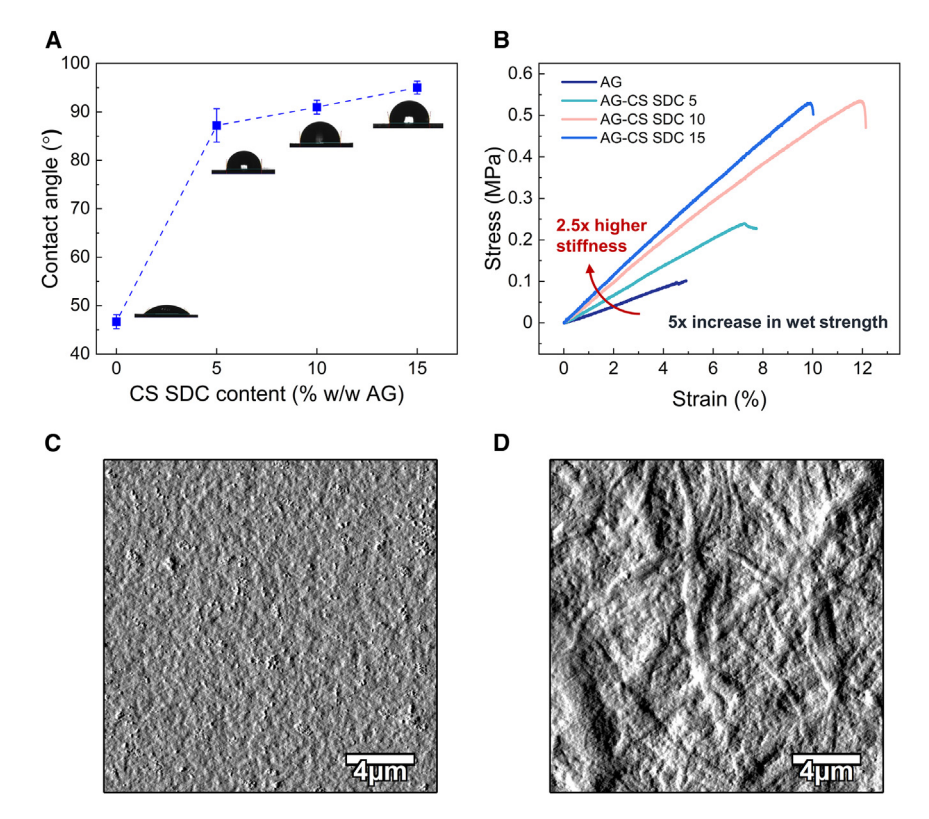


Figure 3. Hydrostability of the AG-CS SDC composite film

(A) Water contact angle of composite film with different loadings of CS SDCs. Insets show images of water droplets on the films' surfaces, illustrating the change in the contact angle. Data are presented as mean  $\pm$  SD, n = 3.

(B) Wet tensile strength of AG-CS SDC film with different contents of CS SDCs.

(C and D) Atomic force microscopy (AFM) amplitude traces showing the smooth surface of the AG film and the rough appearance of the composite film with 15% SDCs.

370–700 nm. The clarity and transmittance of the composite films decreased to some extent with higher contents of CS SDCs due to some degree of hazing. These highly doped composite films are optically translucent and slightly hazy in scattered light, but one can easily see through them (Figure 2F). The relatively high translucency of the composite material can be attributed to the close refractive indices (RIs) of AG and CS (1.335 and 1.523, respectively). Small differences in RI ( $\Delta n \approx 0.2$ ) between the matrix and the filler have been previously shown to result in transparent composites. Additionally, the small cross-sectional diameter of the SDC fibrils (nanometer scale) allows the composite film to remain optically translucent with small hazing even at high SDC loadings.

One of the main weaknesses of most biopolymer materials is their susceptibility to water; therefore, the hydrostability of composite film materials reported here is of prime importance for potential practical applications. The addition of CS SDCs substantially increased the water contact angle of the films. The contact angle of pure hydrophilic AG film was approximately 45°. It significantly increased with the inclusion of SDCs, reaching 95° for the AG-CS SDC 15% film (Figure 3A). One major reason for this hydrophobization could be the charge neutralization within the bulk material. As AG has weak negative charge (typically by remnant sulfate and pyruvate groups on the polymer backbone in the natural material) and CS has moderate positive charge, the resulting composite would overall be less hydrophilic than

#### **Article**



each of the individual components (Figure S4). The intermolecular charge neutralization between the AG medium and CS SDCs is the likely reason for the hydrophobicity rise, as the charged groups within the biopolymer film are the major hydrophilic moieties rendering the material susceptible to water. This increase in measured hydrophobicity could also be partially attributed to the branched morphology of the SDCs, which renders the films' surface chemically heterogeneous and increases the surface asperities with features commensurate in size to the largest fibrils in the SDC backbones, as seen with atomic force microscopy (Figures 3C and 3D).

In addition to increasing the surface hydrophobicity of the composite films, the incorporation of CS SDCs inside the AG matrix improves the mechanical properties of the wet films compared to the pure AG matrix. The wet AG films displayed only a small elastic region followed by a plastic region. The addition of 15 wt % CS SDCs inside the AG matrix increased the wet tensile strength by  $\sim 5\,\mathrm{x}$  to reach about 0.6 MPa (Figure 3B). This increase in wet strength shows that even though the hydrogen bonds between the AG and CS SDCs could be disrupted in the presence of water, the swollen CS SDC network could still offer some degree of reinforcement to the AG matrix. Additionally, the Young's modulus in the wet-film state increases from 2.2 MPa for the pure AG film to 5.75 MPa for AG-CS SDC 15 film. While these values for wet mechanical properties of the AG-CS SDC composite films need further improvement, they are comparable to those of previously reported cellulose-based materials in the wet state.  $^{54,55}$ 

#### Structure-property relationships

Both AG and CS contain a large number of functional groups such as hydroxyl and amino groups, which are expected to establish prolific hydrogen bonds within the material (Figure 4A). Fourier transform infrared (FTIR) spectra were used to identify the H-bond interactions between AG and CS SDCs. Pure AG shows the typical stretching vibrations of OH groups ( $\nu_{O-H}$ ) centered around 3,374 cm<sup>-1</sup>. As the CS SDC content increased, an obvious blueshift of  $\nu_{O-H}$  was observed from 3,381 cm<sup>-1</sup> for AG-CS SDC 5 to 3,390 cm<sup>-1</sup> for AG-CS SDC 15 (Figure 4B). This confirms the formation of numerous H-bonds between the hydroxyl groups on both AG and glycerol molecules and the hydroxyl and amino groups on the CS surface. Such strong intermolecular hydrogen bonds at the interface between the AG and the CS SDC networks could play a key role in the reinforcement effect seen with the addition of SDCs.

The reinforcement role of the fibrillar SDCs is evidenced by scanning electron microscopy (SEM) observation of the fractured surfaces of the AG and AG-CS SDC 15% films after tensile testing. These observations show distinct differences in the fracture morphologies (Figure 4C). The pure AG film showed large open spaces in the fracture crack. On the other hand, the fractured AG-CS composite reveals a network of extended fibrous SDCs in the fracture zone, demonstrating the reinforcing role of the SDCs. The AG-CS SDC film showed no separation between the AG matrix and the CS SDCs, pointing out the high adhesion between their interfaces. The presence of an intertwined fibrous network and its strong anchoring due to abundant H-bonds are possibly major contributors to the outstanding mechanical reinforcement effect of the SDCs.

In order to examine the effect of SDC addition on the viscoelastic behavior of the composite films, we investigated their complex moduli ( $G^*$ ) and loss tangent (tan  $\delta$ ) as a function of frequency. Both  $G^*$  of the AG-CS SDCs and the AG films showed minimal dependance on frequency as expected for these solid-like



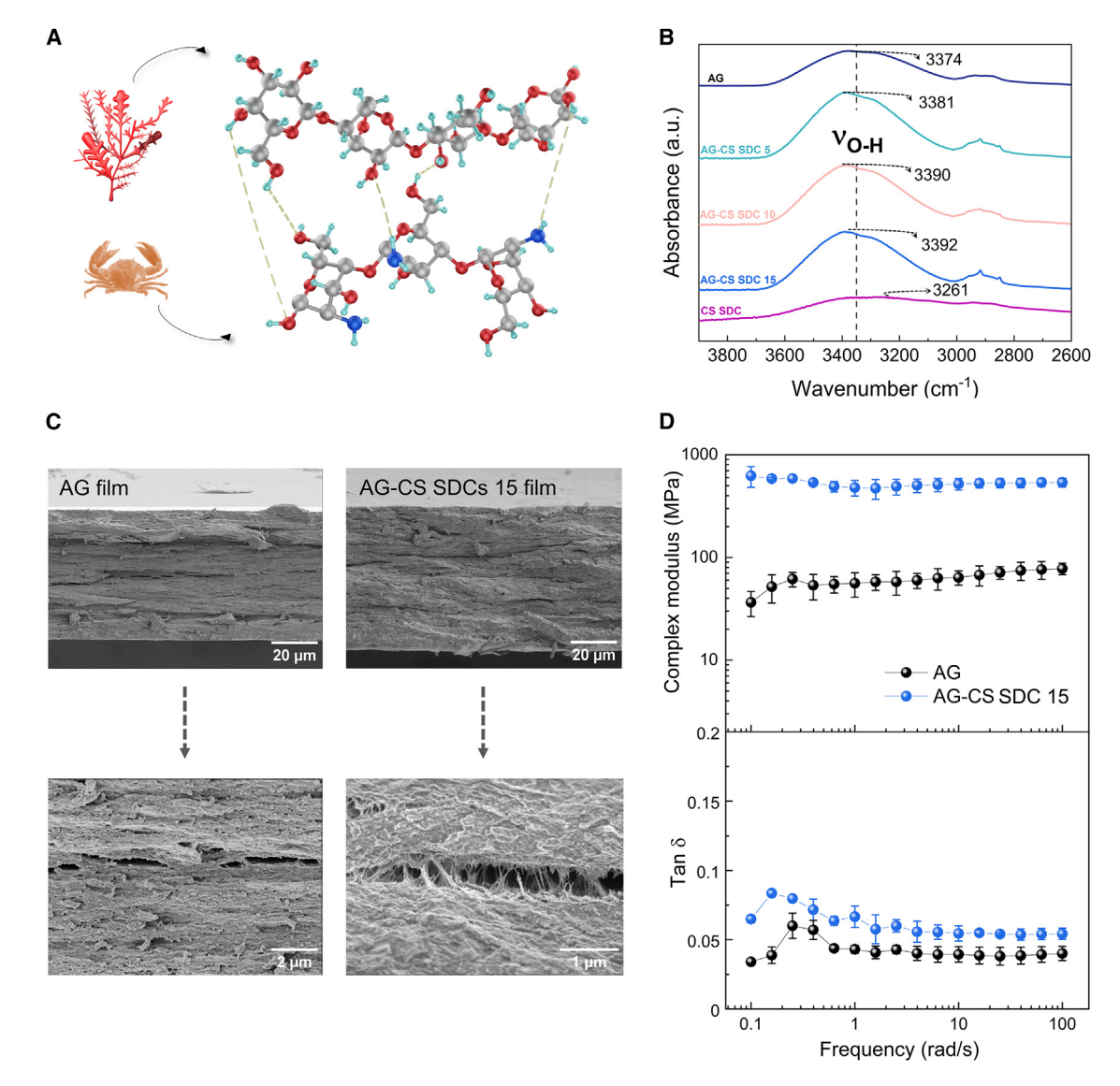


Figure 4. Reinforcement mechanism of CS SDCs inside the AG matrix

(A) Schematic of H-bond interactions (dotted lines) taking place between the AG molecules derived from red seaweed and CS molecules derived from crustaceans.

- (B) FTIR spectra of AG, CS SDC, and AG-CS SDC composites showing the O-H stretching vibration variation with the CS SDC content.
- (C) SEM images of the fracture surfaces of AG film (top) and AG-CS SDC 15 film (bottom).

(D) Frequency dependance of the complex modulus and  $\tan\delta$  of AG and AG-CS SDC 15 films by dynamic mechanical analysis (DMA). Data are presented as mean  $\pm$  SD, n=3.

structures (Figure 4D). The SDC inclusion in the AG-CS SDC 15 film has a significant reinforcement effect characterized by more than one decade increase in G\* compared to the pure AG film. The larger G\* for the composite film suggests higher interactions between the AG and the CS SDCs as well as larger viscous dissipative ability. Tan  $\delta$  increases with the addition of SDCs in the AG matrix, indicating a highly efficient energy dissipation mechanism with the SDCs.  $^{56}$  This unique feature of the SDC reinforcement network enables the local dissipation of high stresses that would otherwise cause the pure AG film to fracture, simultaneously endowing the composite film with excellent toughness and strength.



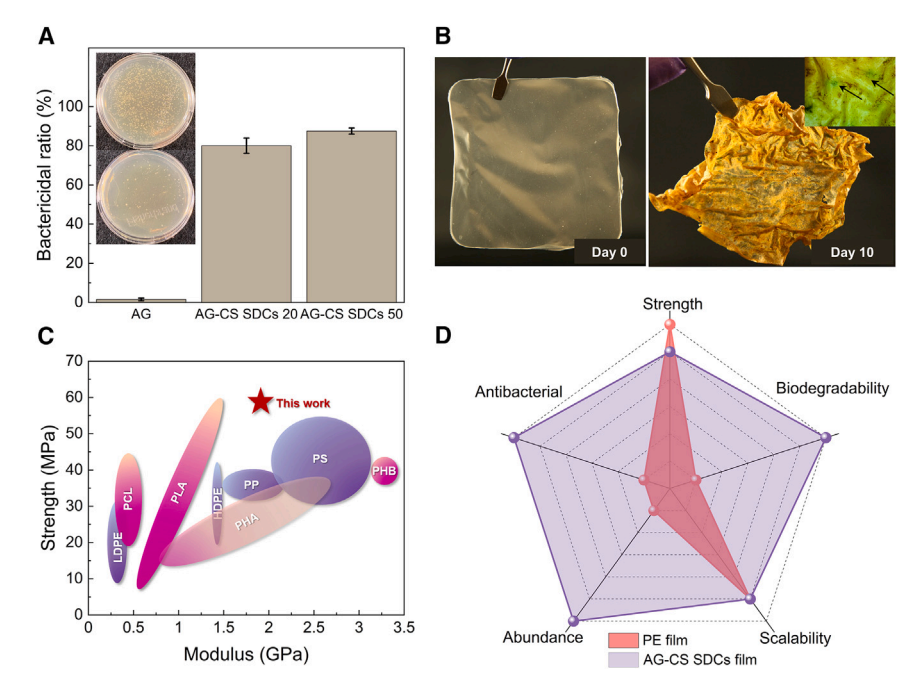


Figure 5. Antibacterial properties and biodegradability of AG-CS SDC composite films and comparison of their mechanical properties with other plastics

(A) Bactericidal effect of AG-CS SDC films compared to the pure AG film. Inset shows photographs illustrating the number of colony-forming units for pure AG film (top) and AG-CS SDC 20 film (bottom). Data are presented as mean  $\pm$  SD, n = 3.

(B) Photographs of an AG-CS SDC 15 film before and after being buried in soil for 10 days. (C) Ashby-type diagram of tensile strength vs. elastic modulus of AG-CS SDC 30 film compared with some common unreinforced petroleum-based as well as biobased plastics. LDPE and HDPE, low-and high-density polyethylene<sup>60</sup>; PCL, polycaprolactone<sup>61</sup>; PLA, polylactic acid<sup>62</sup>; PHA, polyhydroxyalkanoates<sup>62</sup>; PP, polypropylene<sup>60</sup>; PS, polystyrene<sup>60</sup>; PHB, poly(3-hydroxybutyrate). (D) Semi-qualitative radar plot comparing the various functional aspects of the AG-CS SDC film reported here and commercial (potentially reinforced) PE plastic films.

#### Antibacterial properties and biodegradability

The potential utilization of these sustainable composites in applications such as food and consumer packaging could be further enhanced if they have antibacterial properties. CS has been previously shown to be an antibacterial agent due to the surface interactions between its molecular chains and microbial cell walls.<sup>57</sup> While the details of the mechanism behind the antimicrobial activity of CS are still being investigated, it has been attributed to ionic bonding between the positively charged CS and the outer membrane layer on the cell wall. This disrupts cell function and blocks the transport of nutrients, ultimately leading to cell death. 58,59 The bactericidal activity of our films was investigated against E. coli as one of the most common gram-negative pathogens. The films made of pure AG did not show any antibacterial effect, while, on the other hand, the number of colony-forming units (CFUs) is significantly reduced in the case of the composite film containing 20 wt % CS SDCs. Quantitatively, the bactericidal ratio increases from 1.5% for neat AG film up to 82% for AG-CS SDC 20 film (Figure 5A). This shows that the composite film can effectively prevent the growth of different microbial pathogens by harnessing the properties of its natural CS component (CS being locally separated in the SDC domains, which also produces surface charge inhomogeneity) without the need for any synthetic additives that could affect the biodegradability or biocompatibility of the film.



One further characteristic of the composite films that would be critically important for their potential application is their biodegradability. This property was tested by placing film samples in aerated soil in a controlled lab environment and monitoring the weight changes caused by the material degradation by soil microorganisms. For comparison, a Ziploc bag film of comparable size made of polyethylene (PE) was placed in a similar environment to monitor its weight changes with time over a period of 2.5 months. The weight of the AG-CS SDC 15 film decreased rapidly over the first 10 days, as bacteria and fungi begin to feed on the available nutrients (Figure S5). After 10 days in the soil, fungi growth spots started to appear on the surface of the AG-CS SDC 15% film (Figure 5B). Additionally, the composite film started to break down in different locations, losing its mechanical integrity. Meanwhile, the Ziploc film surface did not show any major morphological changes even after 32 days in the soil (Figure S6). Further, the PE film showed no change in weight over the whole period of testing (Figure S5). It is worth noting that the biodegradability of a material sample in a lab environment may not necessarily reflect the behavior of that material in real-world conditions, which can vary considerably in the presence of other factors, such as UV radiation and other pollutants. However, the results clearly indicate the susceptibility of the AG-CS SDC films to biodegradation in the soil environment, likely as result of a complex process involving enzymatic hydrolysis and microbial degradation. <sup>64,65</sup> It is also interesting to note that these films combine two formally conflicting features—antibacterial activity and biodegradability. However, their bactericidal action is based on a natural polymer, CS, which in the short term is effective toward the specific pathogen tested but in the longer term will be subject to normal enzymatic degradation and microbial ingestion in the soil environment containing a myriad of microorganisms. The combination of short-term bactericidal action and long-term biodegradability of these films reveals numerous advantages against inert non-degradable synthetic plastic packaging and similar materials.

The potential applications of such films include replacement of the commonly and broadly used packaging and structural films from synthetic polymers. In order to achieve this goal, first, the biopolymer composites should possess mechanical characteristics that are comparable to those of the presently used synthetic polymers. We compared the tensile strength and elastic modulus of AG-CS SDC 30 film to the ones of common polymers by plotting our results vs. their literature values in Figure 5C. The plot shows that the AG-CS SDC films have mechanical characteristics that are similar or superior to most common petroleum-based and biobased plastic materials. As our data show, these mechanical characteristics are a direct consequence of the use of the CS SDCs as filler. The hierarchical morphology, high aspect ratio, and enhanced networking of the CS SDCs make them specifically suitable as reinforcing materials. As mentioned earlier, the formation of a tough material is also contingent on the strong interfacial adhesion between the two phases of AG and CS by abundant intermolecular H-bonding interactions. These hydrogen bonds can dissipate energy on a molecular scale during extension by a dynamic formation process.66

The intermolecular charge neutralization between the AG medium and CS SDCs is also of specific interest, as it will lead to densification, hydrophobization, increased hydrostability, and decreased water and oxygen permeability. It is important to note, however, that just ion charge neutralization by molecular mixing of positively and negatively charged biopolymers may lead to "curdling" and clumping by molecular precipitation. The problem is elegantly avoided by the unique morphology of the SDCs reported here. The highly branched hierarchical structure of the SDCs

#### Article



presents enough surface area for matrix interfacing and charge neutralization, while the fibrillar backbone preserves the continuity of the material network and provides mechanical resilience. However, the exact mechanisms by which the AG-CS SDC charge neutralization controls the hydrostability and permeability of the films warrants further investigation.

The potential replacement of the common synthetic polymer films, such as the ones listed in Figure 5C, will further require consideration of a much broader set of features related to their manufacture, application, and externalities. Thus, in conclusion, we seek to compare the broader characteristics of common synthetic plastics and the AG-CS SDCs by constructing the semi-qualitative radar plot shown in Figure 5D. It reflects a few other key features of these materials: (1) AG-CS SDC films are biodegradable in soil environments, without the need for complex or expensive breakdown processes. (2) CS SDCs endow the film with an inherent antibacterial activity without adding non-biodegradable additives. (3) Although the films reported here have good mechanical properties, further development will be needed to match the ones of the best reinforced synthetic films, especially in wet conditions. (4) The SDC fabrication process is scalable and based only on water medium, thus having the additional benefit that the production of such films is simple, does not involve organic solvents, and is benign to the environment.

In conclusion, we report the fabrication of a high-performance composite film based on an AG matrix reinforced with SDCs made of CS. Both AG and CS represent inexpensive, abundant, and renewable resources extracted from marine waste products. Owing to the hierarchically branched nature of the SDCs and their entanglement, the films acquire outstanding functional properties including high strength, high toughness, and hydrophobicity. The mechanical properties are attributed to the extrinsic toughening mechanism enabled by the strong AG-CS SDC interfacial bonding, energy dissipative ability, and extensive H-bonding within the matrix. These biodegradable films also show efficient antibacterial properties and high translucency. Given that such materials can have multiple properties that are comparable or superior to common petroleum-based as well as biobased plastic films, the AG-CS SDC film can become a sustainable alternative material in applications such as food, pharmaceutical, and consumer packaging and in soft electronic substrates. Their manufacture to scale will require the transition from batch-mode solution casting to large-scale fabrication of films by continuous processes such as extrusion and roll drying. While the development of such manufacturing processes is still forthcoming and will require techno-economic and life cycle analyses once the technology implementation is scaled up, the results shown here demonstrate that the reinforcement of biopolymer films with SDCs and other possible fibrillar inclusions can become the basis of a universal strategy for producing sustainably sourced composite films that combine high strength and toughness.

#### **EXPERIMENTAL PROCEDURES**

#### Resource availability

#### Lead contact

Further information and requests for resources and reagents should be directed to and will be fulfilled by the lead contact, Orlin D. Velev (odvelv@ncsu.edu).

#### Materials availability

This study did not generate new unique reagents.



#### Data and code availability

Any additional information required to reanalyze the data reported in this article is available from the lead contact upon request.

#### **Materials**

All chemicals were obtained commercially. AG (marine algae, sulfate  $\leq$  0.15%), CS (shrimp shells, low molecular weight: 50–190 kDa, deacetylation  $\geq$  75%, alpha form), glycerol, sodium citrate dihydrate (NaCit), fluorescein isothiocyanate (Sigma-Aldrich), and acetic acid (Alfa Aesar) were used as received without further purification. Deionized water was used in all experiments (resistivity: 18.2 M $\Omega$  cm).

#### **Fabrication of CS SDCs**

CS was dissolved in 1.5% (v/v) acetic acid at 3 wt %. The solution was stored at  $4^{\circ}$ C until further use. To fabricate CS SDCs, a colloidal high-shear mixer (magic LAB, IKA) was filled with 500 mL of 25 mM NaCit solution as the non-solvent crosslinking medium. 10 mL CS solution was directly injected into the shear zone of the IKA operating at 20,000 rpm. The resulting SDCs were washed  $5\times$  with water to remove excess acetic acid and NaCit. Following washing, the particles were centrifuged and diluted to the desired concentration.

#### Characterization of CS SDC morphology

The morphology of CS SDCs was visualized using optical microscopy (BX-61 Olympus), confocal laser scanning microscopy (Leica SP8), and field-emission SEM (FEI Verios 460L). Before SEM observation, all samples were sputter coated with Au-Pd for 45 s at 11 mA current. For confocal and fluorescence microscopy, particles were labeled with fluorescein isothiocyanate by adding the dye in the CS solution before shear precipitation.<sup>67</sup>

#### **Preparation of AG-CS SDC composite films**

AG-CS SDC composites were fabricated via direct solvent casting. First, AG powder was dissolved in heated water to prepare a 1 wt % solution with the addition of glycerol at 20% (w/w AG) as a plasticizer. Upon cooling, a certain amount of the CS SDC suspension was added to the solution to yield the desired concentration of particles in the final film (5–50 wt %). When the suspension of CS SDCs was mixed with the AG gel precursor solution, the SDCs remain well dispersed and are not able to settle since the AG solution is highly vicious and starts gelling rapidly upon cooling, trapping the dispersed SDCs inside the matrix. The mixtures were poured into Teflon or plastic molds and dried at 25°C and 50% relative humidity (RH) for 24 h. The average thickness of the transparent films was about  $\sim\!\!70~\mu m$ . The films are labeled based on the loading level of CS SDCs.

#### **Characterizations**

Mechanical tests were carried out using a universal testing machine (Instron 5943) equipped with a 1 kN load cell. Samples ( $10 \times 2 \text{ cm}^2$ ) were loaded in the machine with a grip distance of 5 cm and a uniaxial extension rate of 1 mm min<sup>-1</sup> until breakdown. The toughness of the composite films was evaluated via the areal integration of the stress-strain curve. In each case, at least 5 samples were tested to ensure reproducibility.

The chemical compositions were characterized using an attenuated total reflectance (ATR)-FTIR spectrometer (Nicolet 6700). For each sample, 128 scans were acquired after a background correction at a resolution of  $4\,\mathrm{cm}^{-1}$ . The analysis was done using Omnic Spectra software.

#### **Article**



Rheological characterization of the viscoelastic properties of the CS SDC suspension and CS solution was conducted using a rheometer (Discovery HR-2, TA Instruments) equipped with a sandblasted parallel-plate geometry (diameter: 40 mm). Small-amplitude frequency sweeps were performed within the linear viscoelastic regime.

The antibacterial properties of the composites were evaluated by counting the CFUs. The composites sampled were placed in a liquid culture solution containing 20  $\mu$ L bacterial suspension (*E. coli*). The cultures were incubated at 37°C for 6 h, diluted 10<sup>4</sup>×, and coated on LB agar plates. The plates were incubated at 37°C for 6 h, and the CFUs were counted. The bacterial suspension without any sample was used as control. The bactericidal ratio (BR) was calculated as follows: BR = (CFU<sub>control</sub> - CFU<sub>sample</sub>)/CFU<sub>control</sub>.

The transmittance of the samples was measured in the wavelength range 250–800 nm using a UV-vis spectrometer (Jasco V550). Measurements are performed in triplicates. Water contact angles were measured by the sessile drop method using a conventional goniometer setup equipped with a drop shape analyzer (First Ten Angstroms 1000B) with  $\sim\!\!5~\mu L$  droplets. The measurements were replicated three times for each sample.

Dynamic mechanical analysis (DMA) of the dried film samples was carried out using an RSA-G2 analyzer (TA Instruments) in tension mode at 0.05% strain (within the LVE regime). Frequency sweeps were performed in the range of 0.1–100 rad/s (0.015–15.9 Hz).

The biodegradability of the composites was determined by recording the weight changes as a function of burial time in the soil. pH and moisture content of the soil used were 6.81 and 23.6%, respectively. A low-density PE film (commercially obtained as Ziploc) was used as a negative control for biodegradation.

#### SUPPLEMENTAL INFORMATION

Supplemental information can be found online at https://doi.org/10.1016/j.xcrp. 2023.101732.

#### **ACKNOWLEDGMENTS**

The authors thank Dr. Kirill Efimenko and Amr Waly for their help with the DMA experiment and antibacterial testing, respectively. The authors also gratefully acknowledge Dr. Jan Genzer and Dr. Lilian Hsiao for the helpful discussions. This research was supported by grants from the US National Science Foundation, CMMI-2233399 and partially EFMA-2029327, CMMI-1825476, and CMMI-2134664. The work was performed in part at the Analytical Instrumentation Facility (AIF) at North Carolina State University, which is supported by the State of North Carolina and NSF (award no. ECCS-2025064). The AIF is a member of the North Carolina Research Triangle Nanotechnology Network (RTNN), a site in the National Nanotechnology Coordinated Infrastructure (NNCI).

#### **AUTHOR CONTRIBUTIONS**

Y.K.: conceptualization, investigation, writing - original draft, and visualization. O.D.V.: conceptualization, writing - review & editing, and supervision.

#### **DECLARATION OF INTERESTS**

Y.K. and O.D.V. are inventors on a patent application submitted by NC State University that covers synthesis and properties of the biopolymer composite films.



## Cell Reports Physical Science Article

#### **INCLUSION AND DIVERSITY**

We support inclusive, diverse, and equitable conduct, presentation, and reporting of research.

Received: July 1, 2023 Revised: October 30, 2023 Accepted: November 14, 2023 Published: December 11, 2023

#### **REFERENCES**

- Geyer, R., Jambeck, J.R., and Law, K.L. (2017). Production, use, and fate of all plastics ever made. Sci. Adv. 3.
- 2. MacLeod, M., Arp, H.P.H., Tekman, M.B., and Jahnke, A. (2021). The global threat from plastic pollution. Science 373, 61–65.
- Lamb, J.B., Willis, B.L., Fiorenza, E.A., Couch, C.S., Howard, R., Rader, D.N., True, J.D., Kelly, L.A., Ahmad, A., Jompa, J., et al. (2018). Plastic waste associated with disease on coral reefs. Science 359, 460–462.
- Gibb, B.C. (2019). Plastics are forever. Nat. Chem. 11, 394–395.
- Chamas, A., Moon, H., Zheng, J., Qiu, Y., Tabassum, T., Jang, J.H., Abu-Omar, M., Scott, S.L., and Suh, S. (2020). Degradation Rates of Plastics in the Environment. ACS Sustain Chem. Eng. 8, 3494–3511.
- Jambeck, J.R., Geyer, R., Wilcox, C., Siegler, T.R., Perryman, M., Andrady, A., Narayan, R., and Law, K.L. (2015). Plastic waste inputs from land into the ocean. Science 347, 768–771.
- Huang, W., Song, B., Liang, J., Niu, Q., Zeng, G., Shen, M., Deng, J., Luo, Y., Wen, X., and Zhang, Y. (2021). Microplastics and associated contaminants in the aquatic environment: A review on their ecotoxicological effects, trophic transfer, and potential impacts to human health. J. Hazard Mater. 405, 124187.
- 8. Zhu, Y., Romain, C., and Williams, C.K. (2016). Sustainable polymers from renewable resources. Nature *540*, 354–362.
- Rosenboom, J.-G., Langer, R., and Traverso, G. (2022). Bioplastics for a circular economy. Nat. Rev. Mater. 7, 117–137.
- Mohanty, A.K., Vivekanandhan, S., Pin, J.M., and Misra, M. (2018). Composites from renewable and sustainable resources: Challenges and innovations. Science 362, 536–542.
- Otoni, C.G., Azeredo, H.M.C., Mattos, B.D., Beaumont, M., Correa, D.S., and Rojas, O.J. (2021). The Food–Materials Nexus: Next Generation Bioplastics and Advanced Materials from Agri-Food Residues. Adv. Mater. 33, 2102520.
- Hou, Q., Zhen, M., Qian, H., Nie, Y., Bai, X., Xia, T., Laiq Ur Rehman, M., Li, Q., and Ju, M. (2021). Upcycling and catalytic degradation of plastic wastes. Cell Rep. Phys Sci. 2, 100514.
- Ates, B., Koytepe, S., Ulu, A., Gurses, C., and Thakur, V.K. (2020). Chemistry, Structures, and Advanced Applications of Nanocomposites

- from Biorenewable Resources. Chem Rev. 120, 9304–9362.
- Pei, Y., Wang, L., Tang, K., and Kaplan, D.L. (2021). Biopolymer Nanoscale Assemblies as Building Blocks for New Materials: A Review. Adv. Funct. Mater. 31, 2008552.
- Lizundia, E., and Kundu, D. (2021). Advances in Natural Biopolymer-Based Electrolytes and Separators for Battery Applications. Adv. Funct. Mater. 31, 2005646.
- Tardy, B.L., Richardson, J.J., Greca, L.G., Guo, J., Bras, J., and Rojas, O.J. (2022). Advancing bio-based materials for sustainable solutions to food packaging. Nat. Sustain. 6, 360–367.
- Deng, J., Zhu, E.Q., Xu, G.F., Naik, N., Murugadoss, V., Ma, M.G., Guo, Z., and Shi, Z.J. (2022). Overview of renewable polysaccharide-based composites for biodegradable food packaging applications. Green Chem. 24, 480–492.
- **18.** Hillmyer, M.A. (2017). The promise of plastics from plants. Science *358*, 868–870.
- Mekonnen, T., Mussone, P., Khalil, H., and Bressler, D. (2013). Progress in bio-based plastics and plasticizing modifications. J Mater Chem A Mater 1, 13379.
- Georgios, K., Silva, A., and Furtado, S. (2016). Applications of Green Composite Materials. In Biodegradable Green Composites (John Wiley & Sons, Inc)), pp. 312–337.
- 21. Chang, B.P., Mohanty, A.K., and Misra, M. (2020). Studies on durability of sustainable biobased composites: a review. RSC Adv. 10, 17955–17999.
- Papadopoulou, E.L., Paul, U.C., Tran, T.N., Suarato, G., Ceseracciu, L., Marras, S., d'Arcy, R., and Athanassiou, A. (2019). Sustainable Active Food Packaging from Poly(lactic acid) and Cocoa Bean Shells. ACS Appl. Mater. Interfaces 11, 31317–31327.
- Guan, Q.-F., Yang, H.-B., Han, Z.-M., Ling, Z.-C., and Yu, S.-H. (2020). An all-natural bioinspired structural material for plastic replacement. Nat. Commun. 11, 5401.
- Mohammadi, P., Aranko, A.S., Landowski, C.P., Ikkala, O., Jaudzems, K., Wagermaier, W., and Linder, M.B. (2019). Biomimetic composites with enhanced toughening using silk-inspired triblock proteins and aligned nanocellulose reinforcements. Sci. Adv. 5.
- Aaliya, B., Sunooj, K.V., and Lackner, M. (2021). Biopolymer composites: a review. International Journal of Biobased Plastics 3, 40–84.

- Sharma, B., Malik, P., and Jain, P. (2018). Biopolymer reinforced nanocomposites: A comprehensive review. Mater. Today Commun. 16, 353–363.
- Jagadeesh, P., Puttegowda, M., Mavinkere Rangappa, S., and Siengchin, S. (2021). Influence of nanofillers on biodegradable composites: A comprehensive review. Polym. Compos. 42, 5691–5711.
- Ates, B., Koytepe, S., Ulu, A., Gurses, C., and Thakur, V.K. (2020). Chemistry, Structures, and Advanced Applications of Nanocomposites from Biorenewable Resources. Chem Rev. 120, 9304–9362.
- Wijerathne, B., Liao, T., Ostrikov, K., Ken), and Sun, Z. (2022). Bioinspired Robust Mechanical Properties for Advanced Materials. Small Struct. 3, 2100228.
- Grossman, M., Pivovarov, D., Bouville, F., Dransfeld, C., Masania, K., and Studart, A.R. (2019). Hierarchical Toughening of Nacre-Like Composites. Adv. Funct. Mater. 29, 1806800.
- Roh, S., Williams, A.H., Bang, R.S., Stoyanov, S.D., and Velev, O.D. (2019). Soft dendritic microparticles with unusual adhesion and structuring properties. Nat. Mater. 18, 1315–1320
- 32. Bang, R.S., Roh, S., Williams, A.H., Stoyanov, S.D., and Velev, O.D. (2023). Fluid Flow Templating of Polymeric Soft Matter with Diverse Morphologies. Adv. Mater. 35, 2211438.
- Williams, A.H., Roh, S., Jacob, A.R., Stoyanov, S.D., Hsiao, L., and Velev, O.D. (2021). Printable homocomposite hydrogels with synergistically reinforced molecular-colloidal networks. Nat. Commun. 12, 2834.
- Williams, A.H., Hebert, A.M., Boehm, R.C., Huddleston, M.E., Jenkins, M.R., Velev, O.D., and Nelson, M.T. (2021). Bioscaffold Stiffness Mediates Aerosolized Nanoparticle Uptake in Lung Epithelial Cells. ACS Appl. Mater. Interfaces 13, 50643–50656.
- Salati, M.A., Khazai, J., Tahmuri, A.M., Samadi, A., Taghizadeh, A., Taghizadeh, M., Zarrintaj, P., Ramsey, J.D., Habibzadeh, S., Seidi, F., et al. (2020). Agarose-Based Biomaterials: Opportunities and Challenges in Cartilage Tissue Engineering. Polymers 12, 1150.
- Bertula, K., Martikainen, L., Munne, P., Hietala, S., Klefström, J., Ikkala, O., and Nonappa. (2019). Strain-Stiffening of Agarose Gels. ACS Macro Lett. 8, 670–675.

#### Article



- Wang, H., Qian, J., and Ding, F. (2018). Emerging Chitosan-Based Films for Food Packaging Applications. J. Agric. Food Chem. 66, 395–413.
- 38. Cavallaro, G., Micciulla, S., Chiappisi, L., and Lazzara, G. (2021). Chitosan-based smart hybrid materials: a physico-chemical perspective. J. Mater. Chem. B *9*, 594–611.
- Azmana, M., Mahmood, S., Hilles, A.R., Rahman, A., Arifin, M.A.B., and Ahmed, S. (2021). A review on chitosan and chitosanbased bionanocomposites: Promising material for combatting global issues and its applications. Int. J. Biol. Macromol. 185, 832–848.
- Wu, M., Zhang, Y., Xu, L., Yang, C., Hong, M., Cui, M., Clifford, B.C., He, S., Jing, S., Yao, Y., et al. (2022). A sustainable chitosan-zinc electrolyte for high-rate zinc-metal batteries. Matter 5, 3402–3416.
- Ghasemzadeh, H., Afraz, S., Moradi, M., and Hassanpour, S. (2021). Antimicrobial chitosanagarose full polysaccharide silver nanocomposite films. Int. J. Biol. Macromol. 179, 532–541.
- Hu, Z., Hong, P., Liao, M., Kong, S., Huang, N., Ou, C., and Li, S. (2016). Preparation and Characterization of Chitosan—Agarose Composite Films. Materials 9, 816.
- Felfel, R.M., Gideon-Adeniyi, M.J., Zakir Hossain, K.M., Roberts, G.A.F., and Grant, D.M. (2019). Structural, mechanical and swelling characteristics of 3D scaffolds from chitosanagarose blends. Carbohydr. Polym. 204, 59–67.
- Cao, Q., Zhang, Y., Chen, W., Meng, X., and Liu, B. (2018). Hydrophobicity and physicochemical properties of agarose film as affected by chitosan addition. Int. J. Biol. Macromol. 106, 1307–1313.
- Cao, Z., Gilbert, R.J., and He, W. (2009). Simple Agarose—Chitosan Gel Composite System for Enhanced Neuronal Growth in Three Dimensions. Biomacromolecules 10, 2954–2959.
- 46. Tripathi, A., and Melo, J.S. (2015). Preparation of a sponge-like biocomposite agarose– chitosan scaffold with primary hepatocytes for establishing an in vitro 3D liver tissue model. RSC Adv. 5, 30701–30710.
- 47. Taghizadeh, M.T., Ashassi-Sorkhabi, H., Afkari, R., and Kazempour, A. (2019). Cross-linked chitosan in nano and bead scales as drug

- carriers for betamethasone and tetracycline. Int. J. Biol. Macromol. *131*, 581–588.
- Fan, W., Yan, W., Xu, Z., and Ni, H. (2012). Formation mechanism of monodisperse, low molecular weight chitosan nanoparticles by ionic gelation technique. Colloids Surf. B Biointerfaces 90, 21–27.
- Shu, X. (2001). Novel pH-sensitive citrate crosslinked chitosan film for drug controlled release. Int J Pharm 212, 19–28.
- Han Lyn, F., Tan, C.P., Zawawi, R.M., and Nur Hanani, Z.A. (2021). Enhancing the mechanical and barrier properties of chitosan/graphene oxide composite films using trisodium citrate and sodium tripolyphosphate crosslinkers. J. Appl. Polym. Sci. 138, 50618.
- El-Hefian, E.A., Nasef, M.M., and Yahaya, A.H. (2012). Preparation and Characterization of Chitosan/Agar Blended Films: Part 2. Thermal, Mechanical, and Surface Properties. E-Journal Chem 9, 510–516.
- 52. Ritchie, R.O. (2011). The conflicts between strength and toughness. Nat. Mater. 10, 817–822.
- Liu, Y., Yu, S.-H., and Bergström, L. (2018). Transparent and Flexible Nacre-Like Hybrid Films of Aminoclays and Carboxylated Cellulose Nanofibrils. Adv. Funct. Mater. 28, 1703277.
- 54. Zhou, X., Fu, Y., Chen, L., Wang, R., Wang, X., Miao, Y., Ji, X., Bian, H., and Dai, H. (2020). Diisocyanate modifiable commercial filter paper with tunable hydrophobicity, enhanced wet tensile strength and antibacterial activity. Carbohydr. Polym. 248, 116791.
- Kriechbaum, K., and Bergström, L. (2020). Antioxidant and UV-Blocking Leather-Inspired Nanocellulose-Based Films with High Wet Strength. Biomacromolecules 21, 1720–1728.
- Le Goff, K.J., Gaillard, C., Helbert, W., Garnier, C., and Aubry, T. (2015). Rheological study of reinforcement of agarose hydrogels by cellulose nanowhiskers. Carbohydr. Polym. 116, 117–123.
- Sahariah, P., and Másson, M. (2017). Antimicrobial Chitosan and Chitosan Derivatives: A Review of the Structure–Activity Relationship. Biomacromolecules 18, 3846–3868.
- 58. Eaton, P., Fernandes, J.C., Pereira, E., Pintado, M.E., and Xavier Malcata, F. (2008). Atomic

- force microscopy study of the antibacterial effects of chitosans on Escherichia coli and Staphylococcus aureus. Ultramicroscopy 108, 1128–1134.
- Wang, H., Qian, J., and Ding, F. (2018).
   Emerging Chitosan-Based Films for Food Packaging Applications. J. Agric. Food Chem. 66, 395–413.
- Mangaraj, S., Goswami, T.K., and Mahajan, P.V. (2009). Applications of Plastic Films for Modified Atmosphere Packaging of Fruits and Vegetables: A Review. Food Eng. Rev. 1, 133–158.
- 61. Van de Velde, K., and Kiekens, P. (2002). Biopolymers: overview of several properties and consequences on their applications. Polym. Test. 21, 433–442.
- Farah, S., Anderson, D.G., and Langer, R. (2016). Physical and mechanical properties of PLA, and their functions in widespread applications — A comprehensive review. Adv. Drug Deliv. Rev. 107, 367–392.
- Bugnicourt, E., Cinelli, P., Lazzeri, A., and Alvarez, V. (2014). Polyhydroxyalkanoate (PHA): Review of synthesis, characteristics, processing and potential applications in packaging. Express Polym. Lett. 8, 791–808.
- Sawaguchi, A., Ono, S., Oomura, M., Inami, K., Kumeta, Y., Honda, K., Sameshima-Saito, R., Sakamoto, K., Ando, A., and Saito, A. (2015). Chitosan degradation and associated changes in bacterial community structures in two contrasting soils. Soil Sci. Plant Nutr. 61, 471–480.
- Li, S., Wang, H., Wan, Z., Guo, Y., Chen, C., Li, D., Zhu, M., and Chen, Y. (2022). Strong, Water-Resistant, and Ionic Conductive All-Chitosan Film with a Self-Locking Structure. ACS Appl. Mater. Interfaces 14, 23797–23807.
- 66. Zhang, X., Liu, W., Yang, D., and Qiu, X. (2019). Biomimetic Supertough and Strong Biodegradable Polymeric Materials with Improved Thermal Properties and Excellent UV-Blocking Performance. Adv. Funct. Mater. 29.
- 67. Ge, Y., Zhang, Y., He, S., Nie, F., Teng, G., and Gu, N. (2009). Fluorescence Modified Chitosan-Coated Magnetic Nanoparticles for High-Efficient Cellular Imaging. Nanoscale Res. Lett. 4, 287.